Reaction $\pi^- p \to \pi^- \pi^+ \pi^- p$ at 8 GeV/c

T. Kitagaki, S. Tanaka, H. Yuta, K. Abe, K. Hasegawa, A. Yamaguchi,
T. Nozaki,[a] K. Tamai, T. Maruyama,[b] R. Kikuchi,[c] Y. Unno, and Y. Otani
Tohoku University, Sendai 980, Japan

F. Barreiro,[d] O. Benary,[e] J. E. Brau,[f] R. Dolfini,[g] E. S. Hafen, P. Haridas, D. Hochman,[h]
M. F. Hodous,[i] R. I. Hulsizer, V. Kistiakowsky, A. Napier,[b] S. Noguchi,[j] S. H. Oh,
I. A. Pless, J. P. Silverman,[k] P. C. Trepagnier,[l] J. Wolfson,[m] Y. Wu,[n] and R. K. Yamamoto
Massachusetts Institute of Technology, Cambridge, Massachusetts 02139

H. O. Cohn
Oak Ridge National Laboratory, Oak Ridge, Tennessee 37830

W. M. Bugg, G. T. Condo, T. Handler, and E. L. Hart
University of Tennessee, Knoxville, Tennessee 37916
(Received 4 January 1982)

Results from a high-statistics experiment involving an exposure of the SLAC 82-in. hydrogen bubble chamber to a beam of 8-GeV/c π^- yielding a final state of $\pi^-\pi^+\pi^- p$ are presented. Copious production of ρ, Δ^{++}, and f is found. Considerable quasi-two-body production in which one particle decays to one of the above resonances is also observed. Some double-resonance production involving baryon and meson resonances is also seen. The production properties of ρ, Δ^{++}, and f mesons are well described by a double-Regge model.

INTRODUCTION

Considerable work has been done in the past on the reaction

$$\pi^- p \to \pi^+ \pi^- \pi^- p \tag{1}$$

at various energies.[1] That work does include some high-statistics experiments. Also a lower-statistics bubble-chamber exposure at 8 GeV/c, reported some time ago,[2] indicated much resonance production, consisting of both two- and three-body enhancements. It is the purpose of this paper to (a) study the production and decay characteristics of these enhancements, (b) verify the results of previous experiments, and (c) search for previously undetected resonances, with the aid of the present experiment, which contains the highest available statistics at 8 GeV/c.

We present a discussion of the experimental procedure in Sec. II. In Sec. III the composition and some of the properties of the final state are discussed. We examine the production mechanisms in the formation of the quasi-three-body states

TABLE I. Topological cross sections.

Prongs	σ (mb)	
2	13.98	± 0.30[a]
Elastic	5.07	± 0.11
4	10.20	± 0.22
6	2.45	± 0.06
8	0.202	± 0.007
10	0.00571	$\pm 0.000\,96$
Total 2 – 10	26.84	± 0.57
0	$\simeq 0.80$[b]	± 0.03
Total	27.64	± 0.57
Total[c]	26.5	± 1.2

[a]This value includes the elastic cross section given below.
[b]Taken from smaller and different partial sample.
[c]Obtained from slope in $d\sigma/dt$ elastic and counter value for σ_{elastic}.

TABLE II. Channel cross sections.

Channel	σ (mb)
$p\pi^-\pi^0$	0.733 ± 0.020
$n\pi^+\pi^-$	0.992 ± 0.026
$p\pi^+\pi^-\pi^-$	1.40 ± 0.04
$p\pi^+\pi^-\pi^-\pi^0$	1.60 ± 0.04
$n\pi^+\pi^+\pi^-\pi^-$	0.929 ± 0.036

 ©1982 The American Physical Society

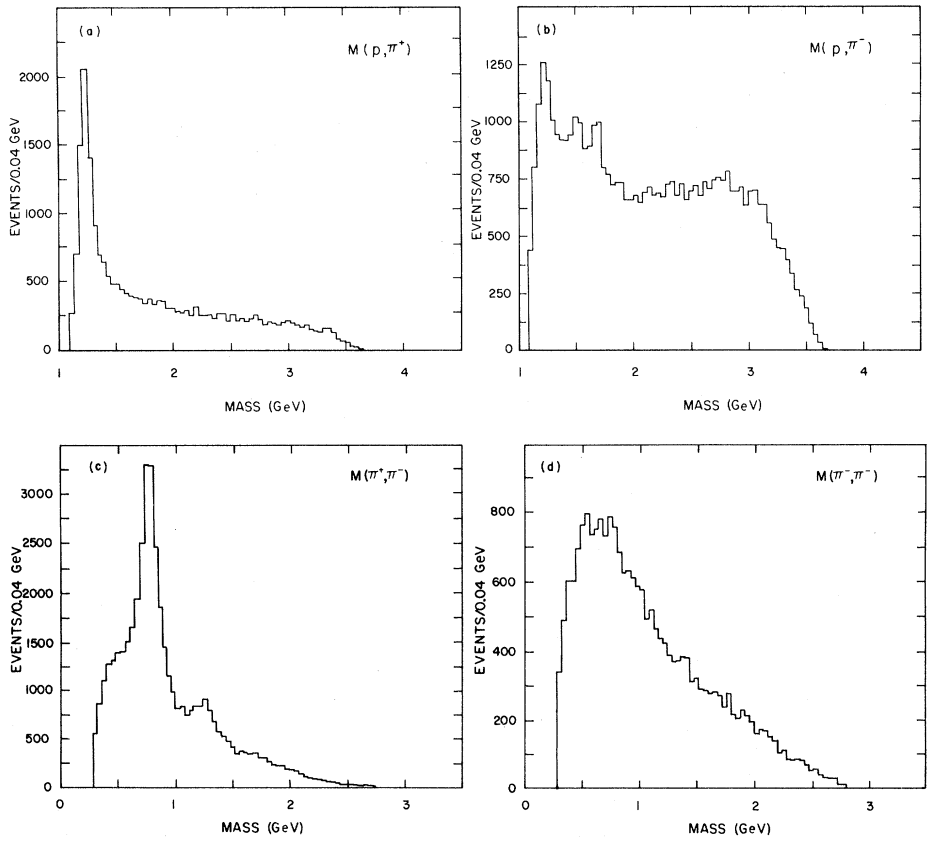

FIG. 1. Effective-mass plots (a) $M(p\pi^+)$, (b) $M(p\pi^-)$, (c) $M(\pi^+\pi^-)$, (d) $M(\pi^-\pi^-)$, (e) $M(p\pi^+\pi^-)$, (f) $M(p\pi^-\pi^-)$, and (g) $M(\pi^+\pi^-\pi^-)$.

$\Delta^{++}\pi^-\pi^-$, $p\rho\pi^-$, and $pf\pi^-$ in Sec. IV. Concluding remarks are given in Sec. V.

II. EXPERIMENTAL PROCEDURES

We have scanned, measured, and analyzed events coming from about 600 000 photographs from the SLAC 82-in hydrogen bubble chamber to an exposure of a beam of 8-GeV/c π^- particles. The measurements were performed by Precision Encoding Pattern Recognition (PEPR) at MIT, by the spiral reader at Tennessee, and by Hough-Powell devices (HPD's) as well as manually at Tohoku. Geometric reconstruction, kinematic fitting, and hypothesis discrimination were handled by the GEOMAT (TVGP)-SQUAW-ARROW program chain. For positive particles whose lab momentum did not exceed 1.2 GeV/c, discrimination between protons and pions was performed.

From a subsample of our events for all multiplicities (about 140 000 events) except zero prongs we have evaluated the total cross section for 2–10 prongs (see Table I). After adding to this the zero-prong cross section from a different smaller sample we obtain $\sigma_{\text{total}} = 27.6 \pm 0.6$ mb consistent with results from counter experiments[3] (viz. 27.5 ± 0.3 mb). As a check on the consistency of our procedure, we have calculated the total cross section, using the slope in four-momentum transfer t of elastic scattering, the counter-experiment value of 4.7 ± 0.1 mb for the elastic cross section, and the optical theorem. Our result (26.5 $\pm$ 1.2 mb) agrees within errors with our other evaluation. The topological cross sections are given in Table I.

In the two- and four-prong samples we have evaluated the four-constraint and one-constraint nonstrange cross sections and have presented them in Table II. All events satisfying four-constraint hypotheses with $\chi^2 \leq 30$ were considered in our evaluation. Among the one-constraint hypotheses about 10% of the events were ambiguous; that is, they satisfied each one-constraint hypothesis. These events were resolved on the basis of peripherality, viz., the hypothesis with the baryon whose value of rapidity was the smallest was

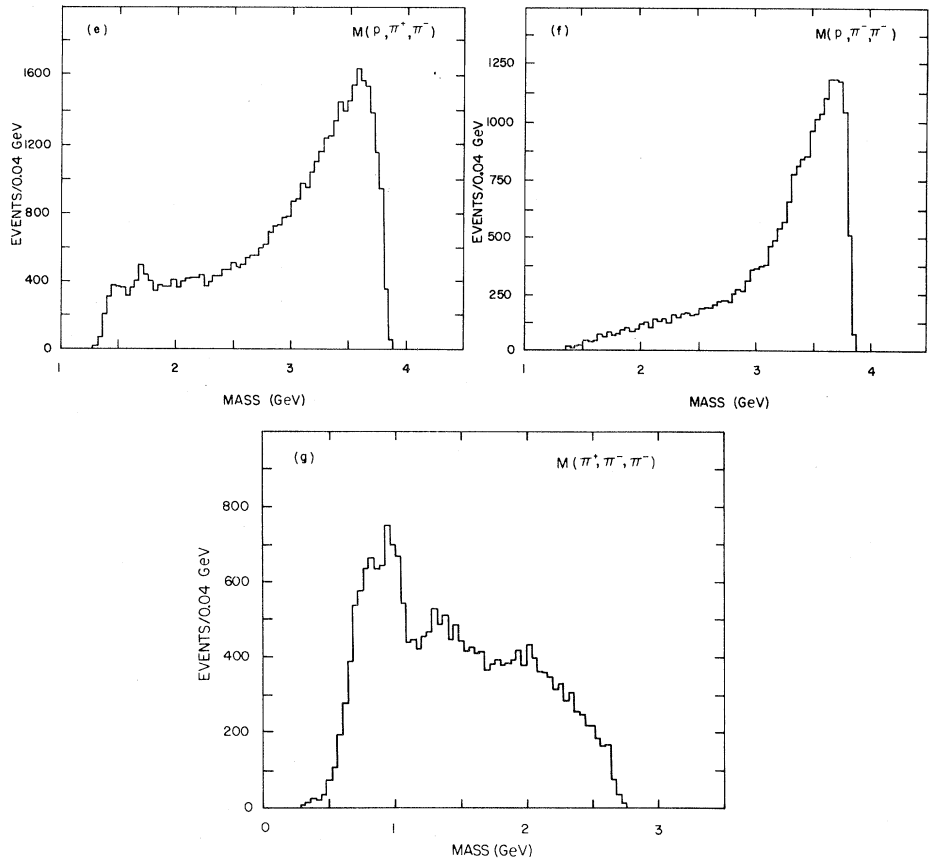

FIG. 1. *(Continued.)*

selected. This procedure was checked by examining the effective mass of final-state particles in which one positive particle had the incorrect mass assigned to it. No bumps in the "wrong" channel were found. The final sample of one-constraint events in two and four prongs were required to have a χ^2 probability $\geq 5\%$ and a missing mass squared between -0.2 and 0.2 GeV^2 for final states having a π^0 and between 0.36 and 1.30 GeV^2 for the final states having a proton and neutron, respectively. The final sample for the four-prong, four-constraint hypothesis was purified by requiring the χ^2 probability $\geq 1\%$ and the missing mass squared between -0.02 and 0.02 GeV^2. The cross sections in Table II were evaluated with corrections for these cuts. This procedure yielded 22 040 events of reaction (1), which represents the experiment with the highest statistics to date at this energy.

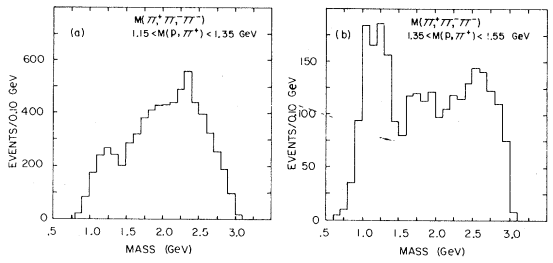

FIG. 2. Effective mass of three-pion system for (a) $1.15 M \leq M(p\pi^+) \leq 1.35$ GeV and (b) $1.35 \leq M(p\pi^+) \leq 1.55$ GeV.

III. RESONANCE PRODUCTION AND DECAY

We present in Fig. 1 our two- [Figs. 1(a)—(d)] and three- [Figs. 1(e)—1(g)] body effective-mass plots. The $p\pi^+$ spectrum is dominated by the Δ^{++} (1236). The $p\pi^-$ distribution, as all distributions involving one of the two π^-'s in the final state, has two combinations for each event. We see in Fig. 1(b) three bumps above a large uniform background. Those bumps in fact correspond to

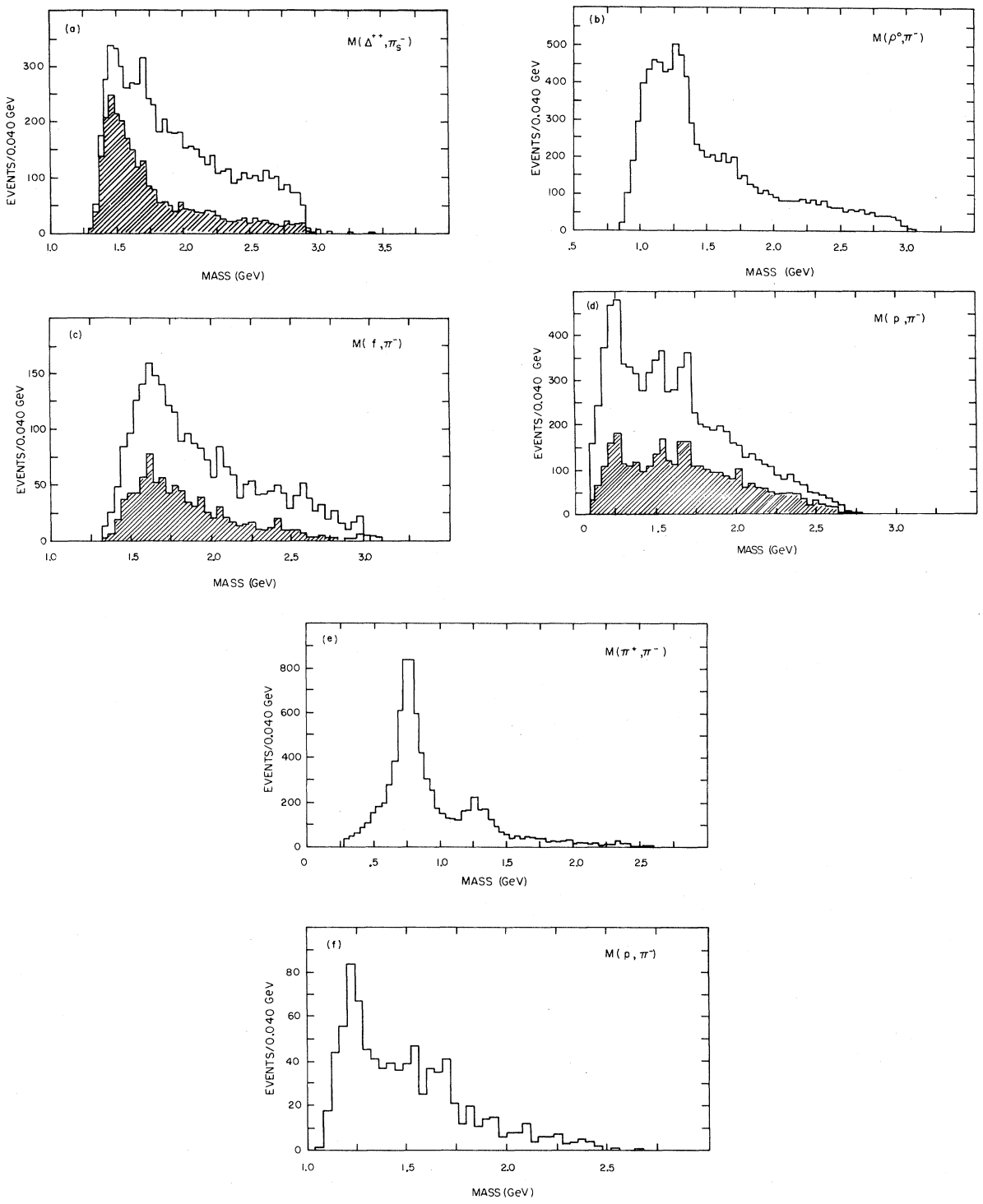

FIG. 3. Effective-mass distributions involving resonances (a) $M(\Delta^{++}\pi_s^-)$, cross-hatched histogram for $|t_{\pi^-,\pi_f^-}| \leq 0.25$ GeV^2, and no ρ produced, (b) $M(\rho^0\pi^-)$ with no Δ^{++} produced, (c) $M(f\pi^-)$ with no Δ^{++} produced, cross-hatched histogram with $|t'_{p,p}| < 0.25$ GeV^2, (d) $M(p\pi^-)$, with no Δ^{++} produced and $|t'_{p,(p\pi^-)}| < 0.5$ GeV^2, lower histogram with ρ^0 at meson vertex, (e) $M(\pi^+\pi^-)$ with no Δ^{++} produced and $|t'_{p,p\pi^-}| < 0.5$ GeV, and (f) $M(p\pi^-)$ with no Δ^{++} produced, no ρ^0 produced, $|t'_{p,p\pi^-}| < 0.5$ GeV^2, and f produced at meson vertex.

TABLE III. Cross sections for resonance production.

Channel	M_0 (MeV)	Γ (MeV)[a]	σ (mb)	Decay
$\rho^0\pi^- p$	766±2	150	0.363±0.047	$\rho^0\to\pi^+\pi^-$
$\Delta^{++}\pi^-\pi^-$	1229±1	123	0.248±0.022	$\Delta^{++}\to p\pi^+$
$f\pi^- p$	1281±6	180	0.052±0.021	$f\to\pi^+\pi^-$
$\Delta^0\pi^+\pi^-$	1229[a]	123	0.044±0.012	$\Delta^0\to p\pi^-$
$N^{*0}(1520)\pi^+\pi^-$	1520[a]	150	0.025±0.016	$N^{*0}(1520)\to p\pi^-$
$N^{*0}(1688)\pi^+\pi^-$	1688[a]	150	0.032±0.015	$N^{*0}(1688)\to p\pi^-$
$\rho^0\Delta^0$			0.035±0.005	
$\rho^0 N^{*0}(1520)$			0.027±0.008	
$\rho^0 N^{*0}(1688)$			0.032±0.009	
$f\Delta^0$			0.019±0.007	
pA_1	1086±12	300	0.211±0.022	$A_1\to\rho^0\pi^-$
pA_2	1286±6	100	0.065±0.009	$A_2\to\rho^0\pi^-$
pA_3	1626±13	300	0.087±0.013	$A_3\to f\pi$
$\pi^- N^{*++}(1470)$	1452±9	200	0.111±0.013	$N^{*++}(1470)\to\Delta^{++}\pi^-$
$\pi^- N^{*++}(1688)$	1687±13	150	0.038±0.009	$N^{*++}(1688)\to\Delta^{++}\pi^-$
Total			1.39±0.05	
$\rho^{0\,b}$			0.733±0.038	
$\Delta^{++\,b}$			0.397±0.016	
f^b			0.158±0.015	
$\Delta^{0\,b}$			0.098±0.009	
$N^{*0}(1520)^b$			0.052±0.014	
$N^{*0}(1688)^b$			0.064±0.012	
Total			1.39±0.05	

[a]These values were held fixed during the fit.
[b]These values include decays from higher-mass resonances.

the Δ^0 (1236), $N(1520)$, and $N(1688)$ resonances. The $\pi^+\pi^-$ effective-mass plot [Fig. 1(c)] has a very large contribution from the $\rho(770)$, and a much smaller peak at the $f(1270)$. The $\pi^-\pi^-$ distribution [Fig. 1(d)] is smooth with no discernible peaks, as expected from the quark model.

Turning to the three-body distributions, the two combinations of $p\pi^+\pi^-$ events [Fig. 1(e)] show little structure, although one may discern enhancements at about 1470 and 1690 MeV. No enhancements are evident in the $p\pi^-\pi^-$ spectrum which peaks near the upper edge of phase space [Fig. 1(f)]. Finally, in Fig. 1(g) the three-pion effective mass does show clear peaks. There is a broad low-mass enhancement from about 1.0—1.4 GeV upon which a narrower enhancement centered at about 1.3 GeV is superimposed. We identify these with the A_1 and $A_2(1310)$, respectively. The $A_3(1640)$ is also visible.

In Fig. 2 we plot the 3π mass spectrum for

TABLE IV. Comparison of cross sections (mb) with other experiments at nearby beam momenta.

Momentum (GeV/c)	$p\pi^+\pi^-\pi^-$	$\Delta^{++}\pi^-\pi^-$	$p\rho^0\pi^-$	$\Delta^0\pi^+\pi^-$
6.0	1.39±0.15	0.39±0.07	0.60±0.10	0.04±0.01
6.7	1.30±0.20	0.30±0.08	0.57±0.14	
7.0	1.70±0.20	0.55±0.11	0.38±0.10	
8.0[a]	1.40±0.04	0.40±0.02	0.73±0.04	0.10±0.01
8.0	1.27±0.07	0.32±0.05	0.56±0.04	0.09±0.02
10.25	1.01±0.21	0.10±0.04	0.70±0.10	

[a]This experiment.

TABLE V. Fits to slope of $e^{-b|t|}$ and $e^{-b'|t'|}$ distributions.

Reaction	Particle	b' Slope of t' $(\text{GeV})^2$	Region $(\text{GeV})^2$	χ^2/DF	b Slope of t $(\text{GeV})^{-2}$	Region	χ^2/DF	Mass range (MeV)
$\pi^- p \to p\pi^+\pi_s^-\pi_f^-$	p	6.99±0.19	0.02–2.0	0.707	7.20±0.30	0.06–2.0	0.794	
$\pi^- p \to p\pi^+\pi_s^-\pi_f^-$	π_f^-	5.25±0.18	0.0–2.0	1.652	4.89±0.21	0.02–2.0	1.150	
$\pi^- p \to N^*(1470)\pi_f^-$	$N^*(1470)$	5.63±0.17	0.0–2.0	2.130	5.21±0.20	0.02–2.0	1.192	$1360 \le M \le 1580$
$\pi^- p \to p\rho^0\pi^-$	p	6.62±0.35	0.04–2.0	0.520	5.97±0.44	0.06–2.0	0.680	$660 \le M \le 880$
$\pi^- p \to pf\pi^-$	p	4.16±0.29	0.06–2.0	0.264	3.62±0.61	0.08–2.0	1.716	$1125 \le M \le 1325$
$\pi^- p \to A_1 p$	A_1	4.75±0.45	0.04–2.0	1.790	3.98±0.60	0.08–2.0	0.541	$925 \le M \le 1225$
$\pi^- p \to A_2 p$	A_2	3.27±0.93	0.04–2.0	1.850	3.08±1.15	0.06–2.0	0.592	$1275 \le M \le 1395$
$\pi^- p \to A_3 p$	A_3	5.44±1.01	0.4–2.0	2.497	4.55±1.17	0.06–2.0	1.041	$1500 \le M \le 1800$
$\pi^- p \to \Delta^{++}\pi^-\pi^-$	Δ^{++}	9.02±0.30	0.0–2.0	2.656	5.60±0.97	1.0–2.0	0.891	$1150 \le M \le 1350$
$\pi^- p \to p\rho^0\pi_s^-$	ρ^0	8.41±0.29	0.0–2.0	2.905	2.85±0.90	1.0–2.0	1.249	$660 \le M \le 860$
$\pi^- p \to pf\pi_s^-$	f	6.11±0.52	0.0–2.0	1.439	2.63±1.82	1.2–2.0	1.487	$1125 \le M \le 1325$
$\pi^- p \to \Delta^0\pi^+\pi_s^-$	Δ^0	7.74±0.41	0.02–2.0	2.447	4.18±0.77	0.08–2.0	0.505	$1150 \le M \le 1350$

events having the $p\pi^+$ effective mass $M(p\pi^+)$ in the region of the Δ^{++} [Fig. 2(a)] and in the next higher-mass region [Fig. 2(b)]. We see an excess of events in the 1.3–2.4-GeV mass region when a Δ^{++} is produced, thus implying that this excess might be a kinematic reflection of the Δ^{++}. The peaks around the 1.2 and 1.6 GeV mass region in Fig. 2(b) shows that the A_1, A_2, and A_3 resonance

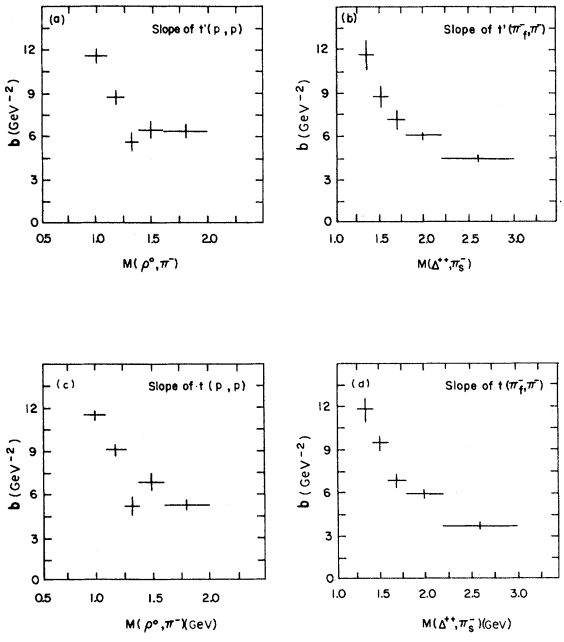

FIG. 4. Slope (b) of t',t distributions for various three-body effective masses, (a) b for $t'_{p,p}$ versus $M(\rho^0\pi^-)$, (b) b for t'_{π^-,π_f^-} versus $M(\Delta^{++}\pi_s^-)$, (c) b for $t_{p,p}$ versus $M(\rho^0\pi^-)$, (d) b for t_{π^-,π_f^-} versus $M(\Delta^{++}\pi_s^-)$.

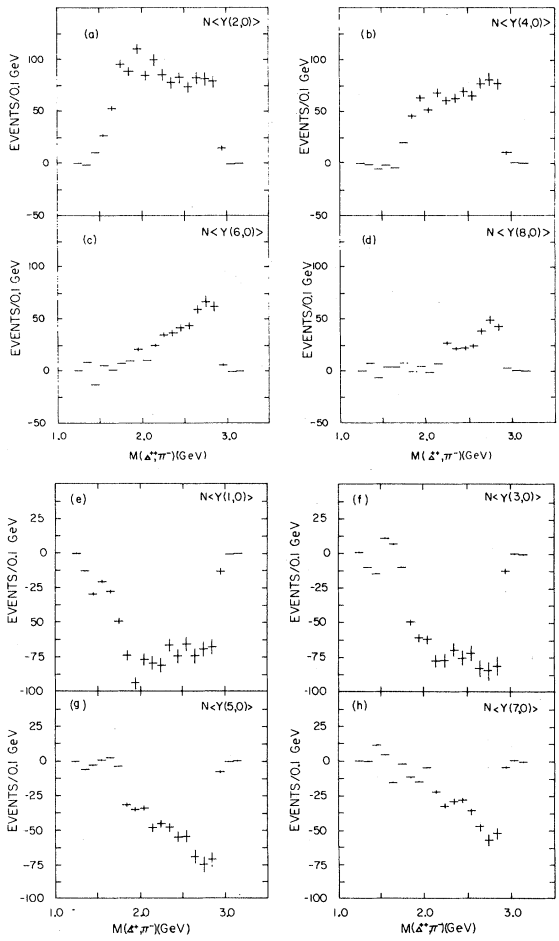

FIG. 5. Unnormalized average moments $N\langle Y_L^0 \rangle$ for various $M(\Delta^{++}\pi^-)$. (a) $N\langle Y_2^0 \rangle$, (b) $N\langle Y_4^0 \rangle$, (c) $N\langle Y_6^0 \rangle$, (d) $N\langle Y_8^0 \rangle$, (e) $N\langle Y_1^0 \rangle$, (f) $N\langle Y_3^0 \rangle$, (g) $N\langle Y_5^0 \rangle$, and (h) $N\langle Y_7^0 \rangle$.

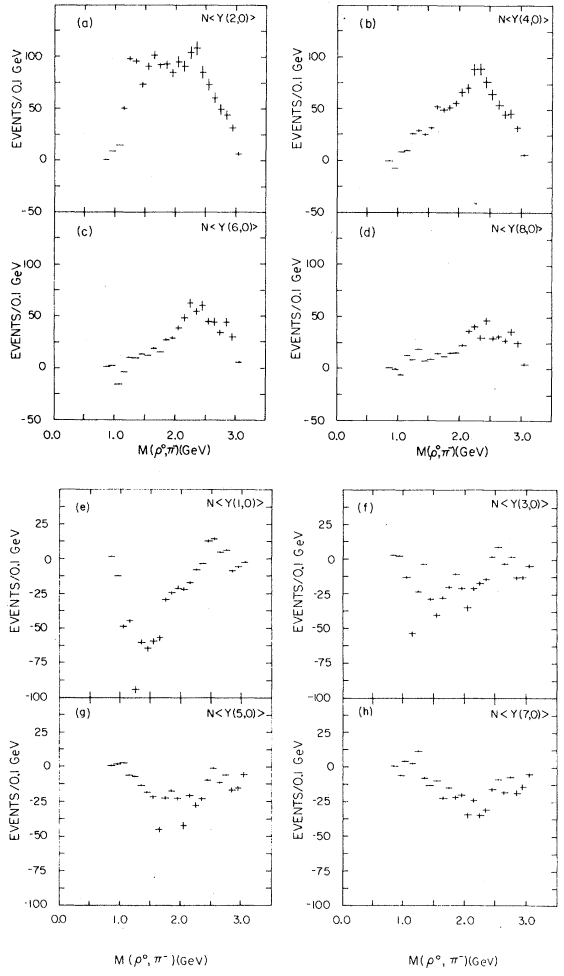

FIG. 6. Unnormalized average moments $N\langle Y_L^0\rangle$, for various $M(\rho^0\pi^-)$. (a)—(h) as in Fig. 5.

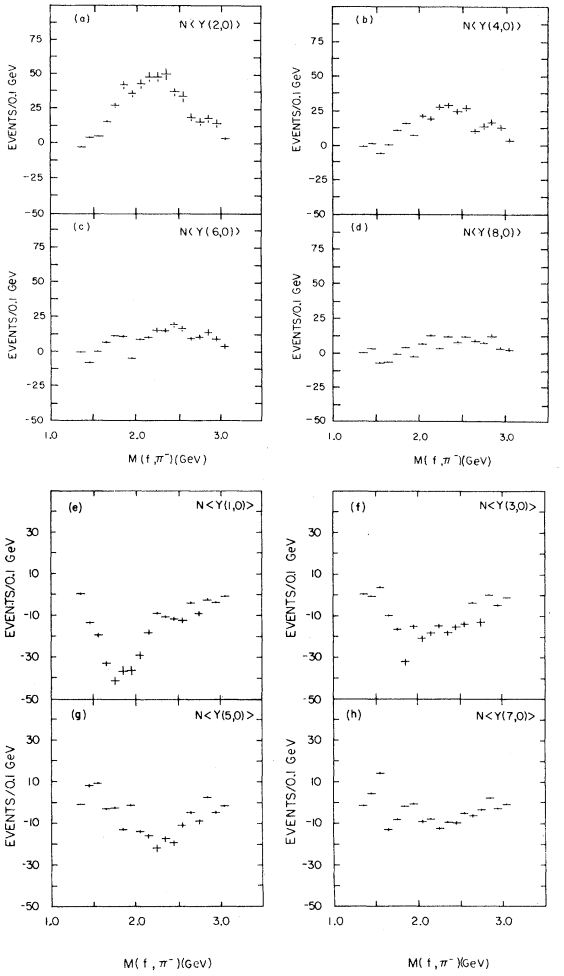

FIG. 7. Unnormalized average moments $N\langle Y_L^0\rangle$, for various $M(f_{\pi}^-)$. (a)—(h) as in Fig. 5.

production dominates in the absence of any competition from Δ^{++} production.

In order to see some of these peaks more clearly and to look for double-resonance production, we have made certain cuts on the data and have illustrated the effective-mass plots in Fig. 3. For this purpose and for later discussion we label each π^- in each event by the subscript s(slow) or f(fast) if the absolute value of t between that π^- and the target proton is less than or greater than that of the other π^-, respectively.

In Fig. 3(a) we have restricted $M(p\pi^+)$ to values $1150 < M(p\pi^+) < 1350$ MeV and have plotted the $M(p\pi^+\pi_s^-)$ effective mass. We see peaks corresponding to the $N(1470)$ and $N(1688)$ resonances which decay to $\Delta^{++}\pi^-$. In the lower histogram are plotted only those events that have no possible ρ^0 contamination and for which $t'=t-t_{\min}$ between the beam and π_f^-, $|t'_{\pi^-,\pi_f^-}| \leq 0.25$ GeV^2. We see that only the $N(1470)$ peak remains.

A ρ meson is taken as that $\pi^+\pi^-$ effective mass for which $660 \leq M(\pi^+\pi^-) \leq 860$ MeV. We have given in Fig. 3(b) the $M(\rho\pi^-)$ spectrum with the restriction of no Δ^{++} production. The A_1 and A_2 are now prominent, but there is little evidence for other enhancements.

The $f\pi^-$ mass distribution [Fig. 3(c)] where f includes events in the range $1125 \leq M(\pi^+\pi^-) \leq 1325$ MeV shows a peak in the A_3 region. We have removed events with possible Δ^{++} production. A large contribution of the events in the A_3 peak have $|t'|_{pp} < 0.25$ GeV^2 indicating peripheral production of A_3 (cross-hatched histogram).

Next we have looked at $M(p\pi^-)$ for which no

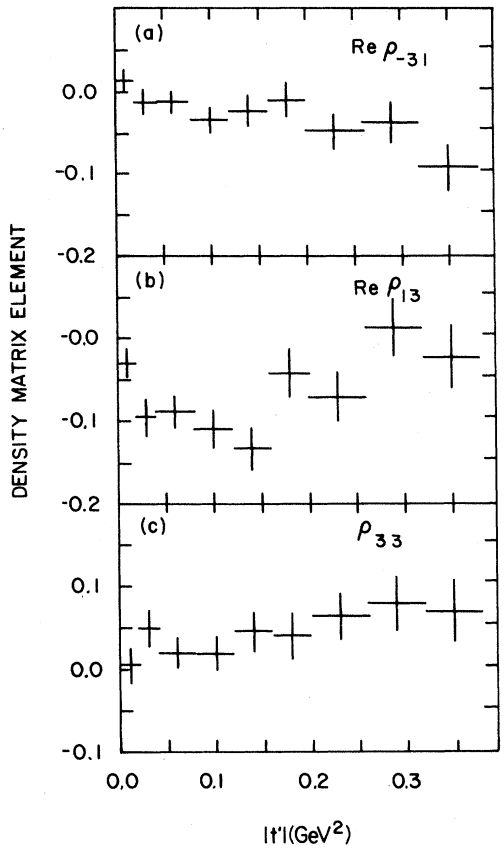

FIG. 8. Density matrix elements of Δ^{++} versus $|t'_{p,\Delta^{++}}|$. (a)Re$\rho_{-3,1}$, (b)Re$\rho_{1,3}$, and (c) ρ_{33}.

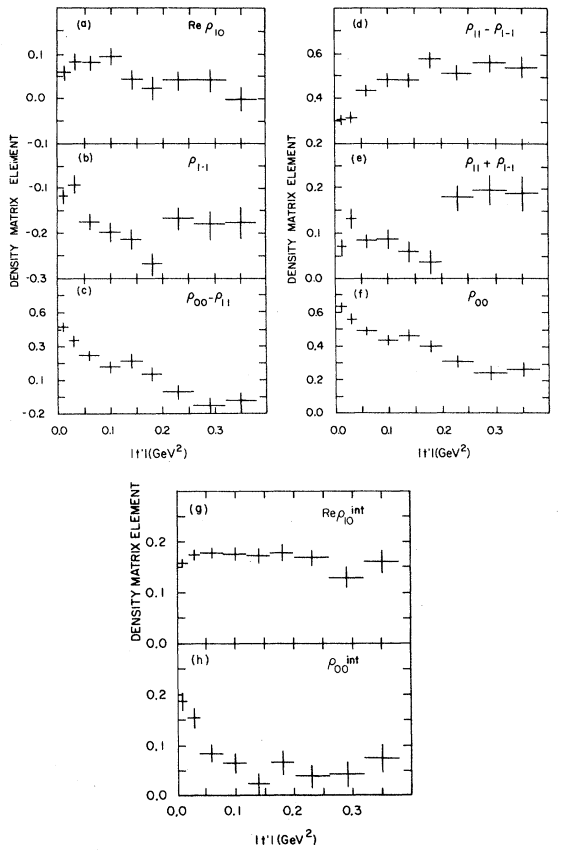

FIG. 9. Density matrix elements of ρ versus $|t'_{\pi^-,\rho^0}|$ (a) Re ρ_{10}, (b) ρ_{1-1}, and (c) $\rho_{00}-\rho_{11}$ all for S-wave background to ρ, and (d) $\rho_{11}-\rho_{1-1}$, (e) $\rho_{11}+\rho_{1-1}$, and (f) ρ_{00} all for assumption of no S-wave background; interference matrix elements (g) Reρ_{10}^{int} and (h) ρ_{00}^{int}.

Δ^{++} production appears and $|t'_{p,(p\pi^-)}| \lesssim 0.5$ GeV^2 [Fig. 3(d)]. We see the $\Delta^0(1136)$, $N(1520)$, and $N(1688)$ bumps well above the background. By restricting the $\pi^+\pi^-$ recoiling off this $p\pi^-$ to have an effective mass in the ρ region, we see in the lower histogram evidence for $\Delta^0\rho$, $N(1520)\rho$, and $N(1688)\rho$ double-resonance production. Conversely, we see ρ and f production in Fig. 3(e) in a sample of events for which there is no Δ^{++} production and for which $|t'_{p,(p\pi^-)}| \leq 0.5$ GeV^2. We have taken the events in the f region of Fig. 3(e), added the restriction that the $M(\pi^+\pi^-)$ combination not lie in the ρ^0 effective-mass region, and

TABLE VI. Cuts on data for double-Regge analysis.

Final state	Exchange	s_1 cut	$M(p\pi^-)$ cut	$\lvert t_1\rvert$ cut	$\lvert t_2\rvert$ cut	Other
$\Delta^{++}\pi^-\pi^-$	π	$\sqrt{s_1} \geq 0.75$ GeV		$\lvert t_1\rvert < 1.0$ GeV^2	$\lvert t_2\rvert < 1.0$ GeV^2	$\phi_H(\Delta^{++}) > 90°$
$\rho p\pi^-$	π	$\sqrt{s_1} > 1.8$ GeV		$\lvert t_1\rvert < 1.0$ GeV^2	$\lvert t_2\rvert < 1.0$ GeV^2	$\lvert t_{\pi^-\rho}\rvert < \lvert t_{\pi^-\pi^-}\rvert$
$\rho p\pi$	ρ	$\sqrt{s_1} \geq 2.2$ GeV	$M(p\pi^-) \geq 1.4$ GeV	$\lvert t_1\rvert < 1.0$ GeV^2	$\lvert t_2\rvert < 1.0$ GeV^2	$\lvert t_{\pi^-\pi^-}\rvert < \lvert t_{\pi^-\rho}\rvert$
$fp\pi$	π	$\sqrt{s_1} \geq 1.4$ GeV		$\lvert t_1\rvert < 1.0$ GeV^2	$\lvert t_2\rvert < 1.0$ GeV^2	$\lvert t_{\pi^-f}\rvert < \lvert t_{\pi^-\pi^-}\rvert$
$fp\pi$[a]	f		$M(p\pi^-) \geq 1.4$ GeV	$\lvert t_1\rvert < 1.0$ GeV^2	$\lvert t_2\rvert < 1.0$ GeV^2	$\lvert t_{\pi^-\pi^-}\rvert < \lvert t_{\pi^-f}\rvert$

[a]Also events with $1150 \leq M(p\pi^+) \leq 1350$ MeV removed.

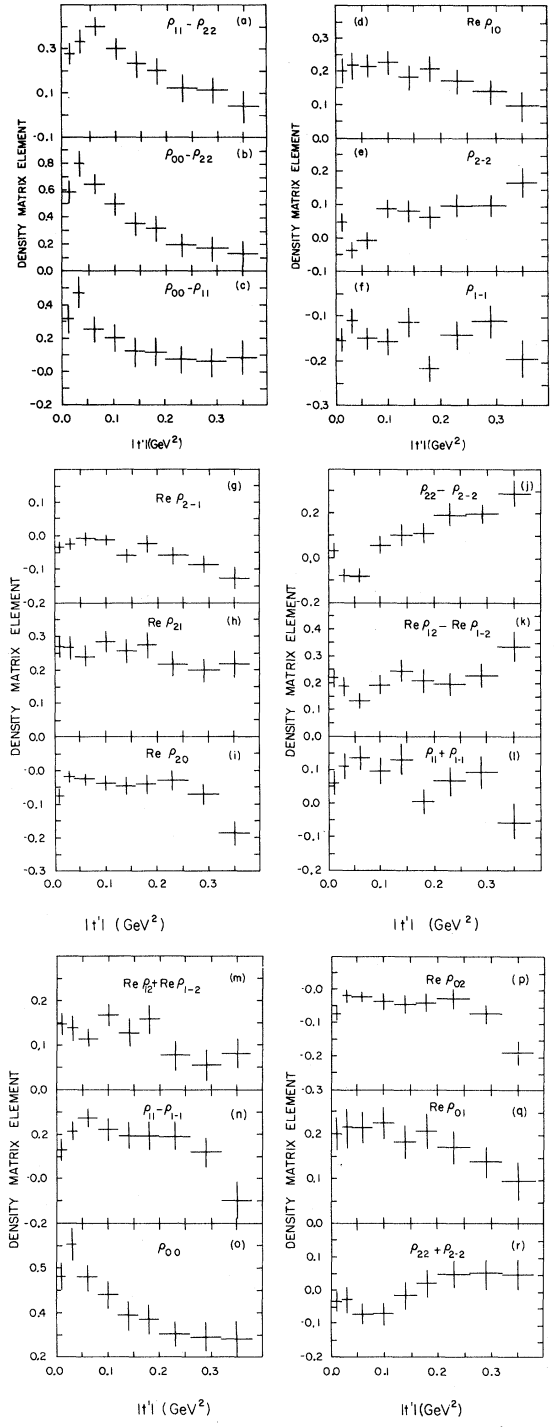

FIG. 10. Density matrix elements of f versus $|t'_{\pi^-,f}|$, not constrained to satisfy positivity. (a)–(i) allowing for the presence of S- and P-wave backgrounds under the f, (j)–(r) with the assumption of pure D wave. (a) $\rho_{11}-\rho_{22}$, (b) $\rho_{00}-\rho_{22}$, (c) $\rho_{00}-\rho_{11}$, (d) Re ρ_{10}, (e) ρ_{2-2}, (f) ρ_{1-1}, (g) Reρ_{2-1}, (h) Reρ_{21}, (i) Reρ_{20}, (j) $\rho_{22}-\rho_{2-2}$, (k) Reρ_{12}−Reρ_{1-2}, (l) $\rho_{11}+\rho_{1-1}$, (m) Reρ_{12} +Reρ_{1-2}, (n) $\rho_{11}-\rho_{1-1}$, (o) ρ_{00}, (p) Reρ_{02}, (q) Reρ_{01}, and (r) $\rho_{22}+\rho_{2-2}$.

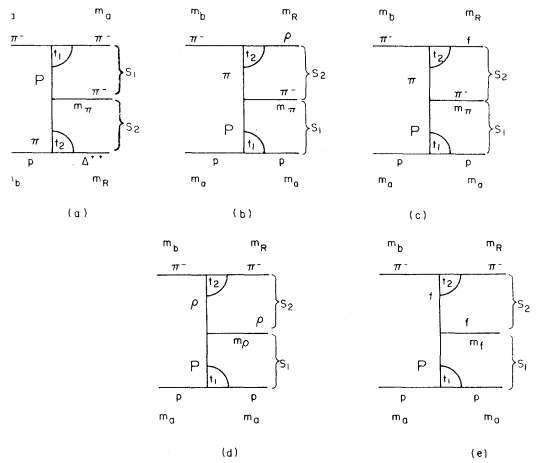

FIG. 11. Reaction diagrams for the double-Regge model. (a) $\pi^-p\to\Delta^{++}\pi^-\pi^-$, (b) $\pi^-p\to\rho\pi^-$, (c) $\pi^-p\to fp\pi^-$, (d) $\pi^-p\to\pi^-\rho p$, and (e) $\pi^-p\to\pi^- fp$.

have plotted the $M(p\pi^-)$ recoiling off of the f in Fig. 3(f). We see $\Delta^0 f$ production as well as hints of $N(1520)f$ and $N(1688)f$ production.

Thus, we have found the considerable number of quasi-two- and quasi-three-body final states listed in Table III with their production cross sections. We note that ρ^0, f, and Δ^{++} production includes decays to these states from higher-mass states. In particular, ρ^0, f, and Δ^{++} production just about saturates the $\pi^-\pi^+\pi^-p$ production cross section.

The cross sections were found by fitting the mass distributions to Breit-Wigner shapes and up to third-order polynomial backgrounds. Mass and four-momentum transfer cuts were imposed on the samples fitted in order to enhance the resonant structures. The effects of these cuts were corrected for in determining the cross sections.

In Table IV we compare some of our results with those at nearby energies. [2,4] We see that the cross sections that we obtain for total Δ^{++}, ρ^0, and Δ^0 production as well as our overall cross section for the channel is within the range of previous results. The mass regions used in our resonance study are listed in Table V.

The peripheral nature of the reaction $\pi^-p\to\pi^-\pi^+\pi^-p$ is illustrated in Table V where we have compiled the values of the slopes of exponential fits to $|t|$ and $|t'|$ distributions in the regions indicated. The values refer to $|t|$ or $|t'|$ with respect to the beam (target) for mesons (baryons). We do note that there is a smaller value for the slope of the A_2 than those for the slope of A_1 or A_3.

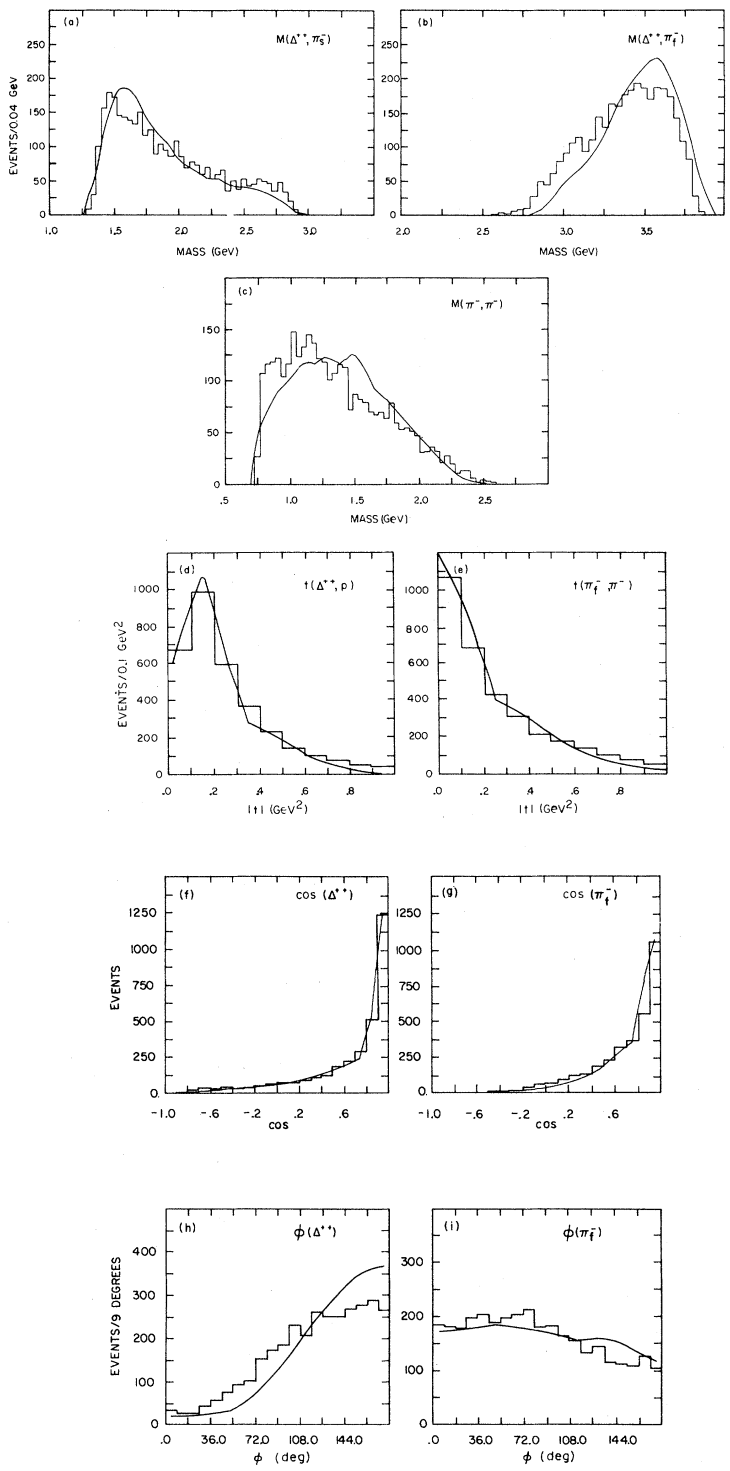

FIG. 12. Comparison of data with double-Regge model, Δ^{++} production with π, P exchanges. Solid curve is model prediction through Fig. 16. (a) $M(\Delta^{++}\pi_s^-)$, (b) $M(\Delta^{++}\pi_f^-)$, (c) $M(\pi^-\pi^-)$, (d) $|t_{p,\Delta^{++}}|$, (e) $|t_{\pi^-,\pi_f^-}|$, (f) $\cos(\Delta^{++})$, (g) $\cos(\pi_f^-)$, (h) $\phi(\Delta^{++})$, and (i) $\phi(\pi_f^-)$.

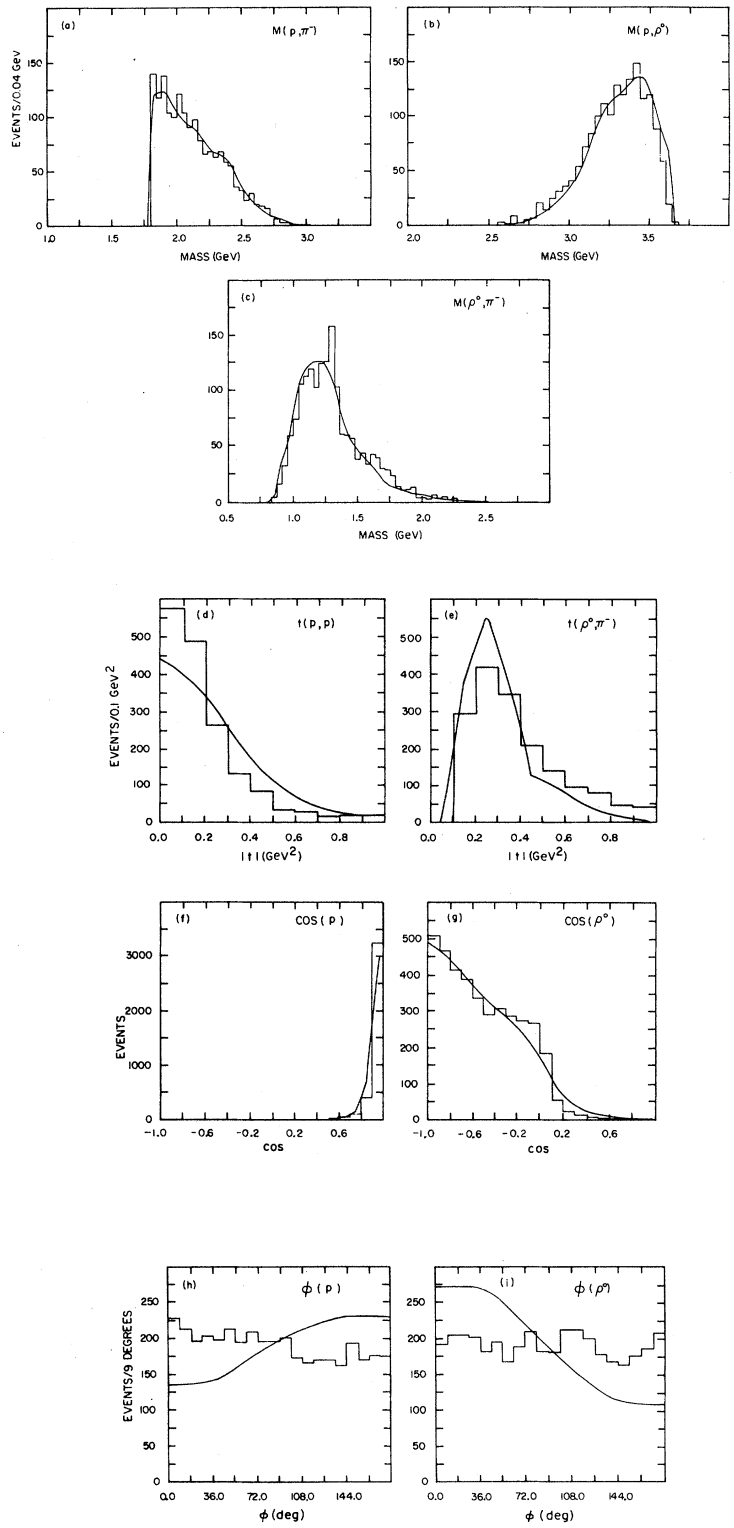

FIG. 13. Comparison of data with model for ρ production with π, P exchanges. (a) $M(p\pi^-)$, (b) $M(p\rho)$, (c) $M(\rho\pi^-)$, (d) $|t_{p,p}|$, (e) $|t_{\pi^-\rho}|$, (f) cos(p), (g) cos(ρ), (h) $\phi(p)$, and (i) $\phi(\rho)$.

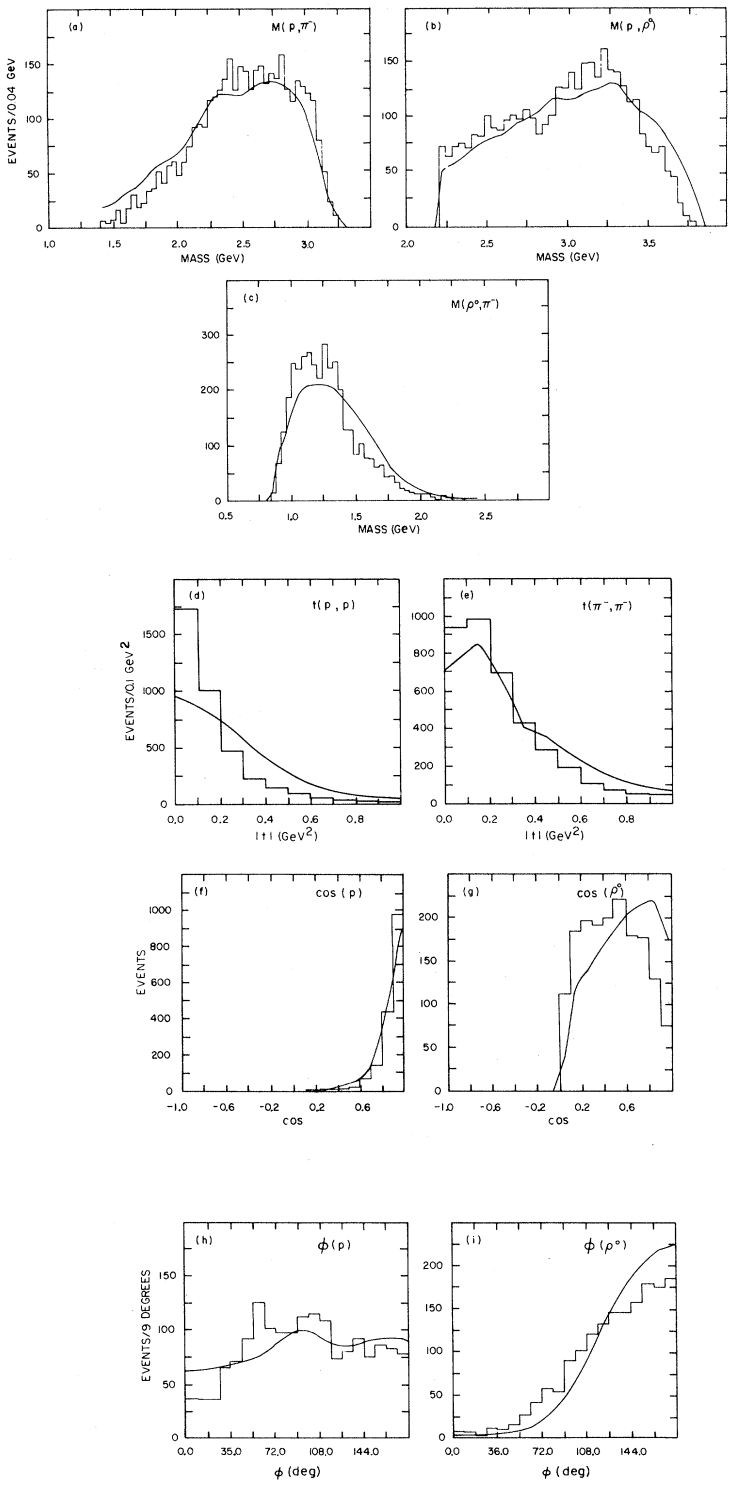

FIG. 14. As in Fig. 13 for ρ, P exchanges, (a)—(d) as in Fig. 13, (e) $|t_{\pi^-,\pi^-}|$, (f) cos(p), (g) cos(ρ), (h) $\phi(p)$, and (i) $\phi(\rho)$.

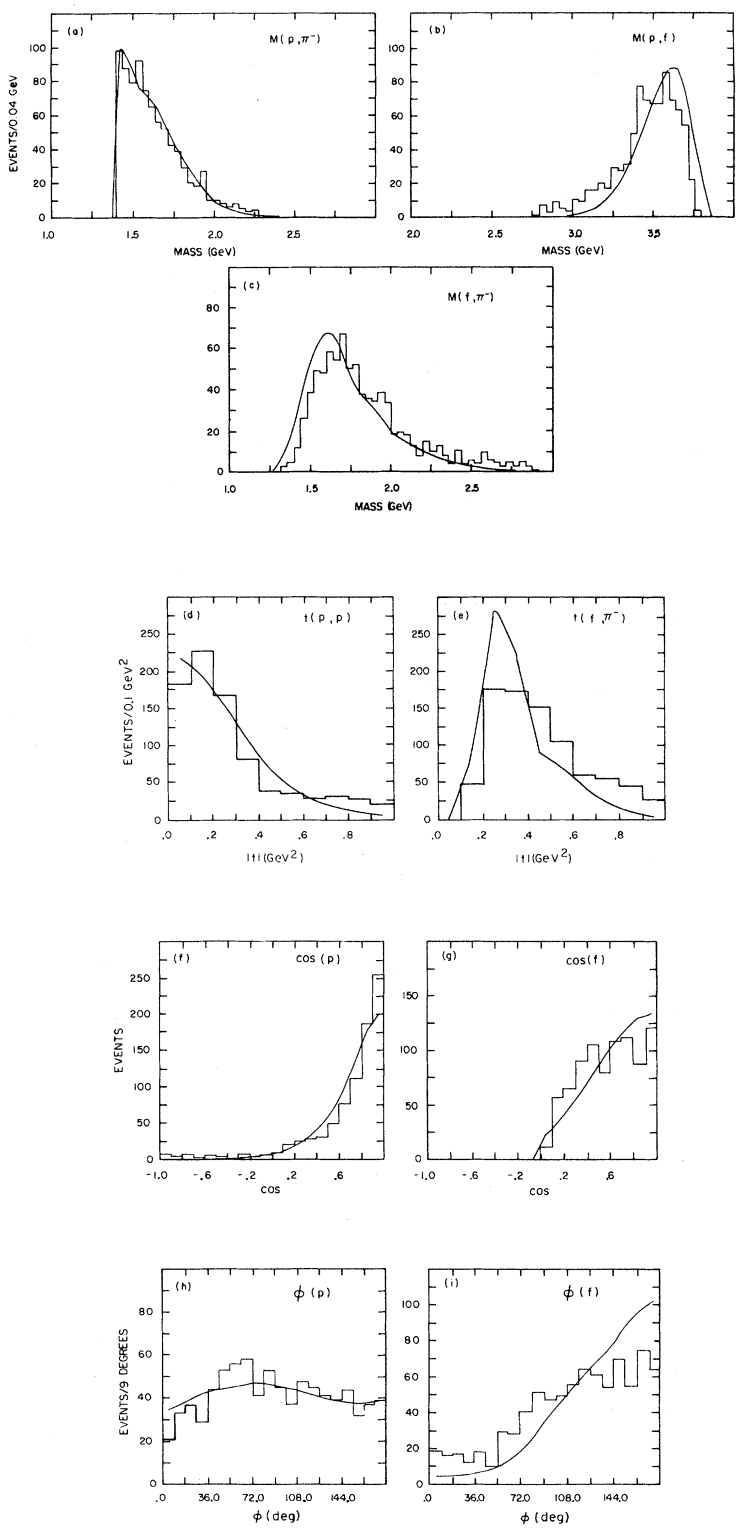

FIG. 15. Comparison of data with model for f production with π, P exchanges. (a) $M(p\pi^-)$, (b) $M(pf)$, (c) $M(f\pi^-)$, (d) $|t_{p,p}|$, (e) $|t_{\pi^-,f}|$, (f) cos (p), (g) cos(f), (h) $\phi(p)$, and (i) $\phi(f)$.

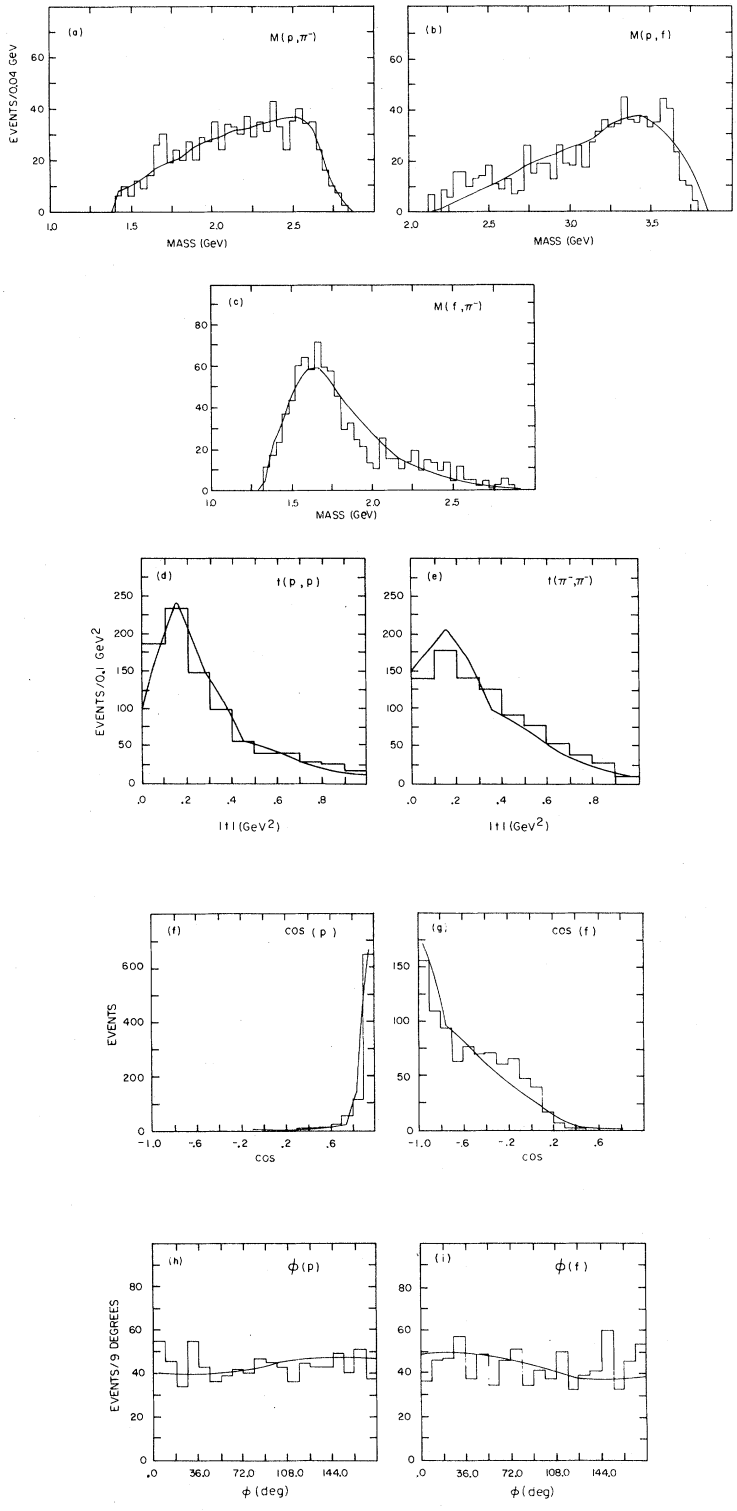

FIG. 16. As in Fig. 15 for f,P exchanges. (a)–(d) as in Fig. 13, (e) $|t_{\pi^-,\pi^-}|$, (f) cos(p), (g) cos(f), (h) $\phi(p)$, and (i) $\phi(f)$.

We have studied the slopes of single diffractive excitation of the beam and target particles as a function of the effective mass of the diffractive excitation. The meson excitation is the $\rho\pi^-$ system and the baryon excitation is the $\Delta^{++}\pi_s^-$ system. The characteristic falloff of the slope with increasing mass is seen in Fig. 4 for both meson and baryon excitations and for both slopes b and b' of $|t|$ and $|t'|$ distributions, respectively. However, whereas the slopes of the baryon excitations monotonically decrease with excitation mass, those of the meson excitations dip at the mass of the A_2, consistent with what was mentioned above. This might be indicative of the A_2 being nondiffractively produced.

It is interesting to study the spin content of these diffractive excitations. This has been done by examining the unnormalized averaged spherical harmonics, $\langle Y_L^0 \rangle \approx \sum_{\text{events}} Y_L^0 (\cos\theta)$ [(where θ is the polar angle of the π_s^- (which is produced with the two-body resonance) in the Gottfried-Jackson rest frame of the excitation], as a function of the excitation mass. We give these values in Figs. 5–7 for $L=1-8$ and with $|t'|$ between the incident or target particle and the meson or baryon resonance, respectively, less than 0.5 GeV^2. Nonzero values for odd moments imply interference between waves of opposite parity whereas nonzero values for even-L moments imply that the spin is at least $L/2$. For the $\Delta^{++}\pi^-$ excitation, Fig. 5, all even moments are small in the $N(1470)$ region consistent with a spin $J \geq \frac{1}{2}$. The $N\langle Y_1^0 \rangle$ distribution suggests that there might be some interference between spin-$\frac{3}{2}$ and spin-$\frac{1}{2}$ states of opposite parity. The excitation near 1700 MeV gives a non-negligible value of $\langle Y_2^0 \rangle$ and possibly $\langle Y_4^0 \rangle$ implying $J \geq \frac{3}{2}$. The odd $\langle Y_L^0 \rangle$ suggest interference between spin-$\frac{3}{2}$ and spin-$\frac{1}{2}$ states, and possibly between spin-$\frac{5}{2}$ and spin-$\frac{3}{2}$ states. The $\rho\pi^-$ excitation (Fig. 6) has a large $L=2$ moment in the A_1-A_2 region and a nonzero $L=4$ moment in the A_2 region consistent with $J \geq 2$ for the A_2. The odd moments indicate interference of spin 1 with spins 0 and 2 in the A_2 region (as background to the A_2). In Fig. 7 we see that $\langle Y_2^0 \rangle$ rises near the A_3 mass, implying $J \geq 1$ for the A_3. There is also indication of spin 0 and 1 interference and spin 0 and 2 interference.

If the Δ^{++}, ρ^0, and f mesons are peripherally produced we may gain some insight into the production mechanism (namely, the t-channel exchange) by examining the density matrix elements. We note that in quasi-two-body production of these resonances where the exchange is between the beam and target vertices of the Feynman diagram, one can discriminate between spin zero and other exchanges by the values of the density matrix elements of the resonance. For quasi-three-body production the exchange is between the vertex containing one incident particle and the resonance and the "effective" vertex containing the other incident particle and the effective two-particle recoil against the resonance. We have used the method of moments to calculate the experimentally accessible density matrix elements as a function of $|t'|$ between the incident particle and the resonance.

We give the results in Fig. 8 for the Δ^{++} from reaction

$$\pi^p \to \Delta^{++}\pi^-\pi^- \,. \tag{2}$$

The density matrix elements have been evaluated in the Gottfried-Jackson frame. The ρ_{33} element is small and fairly uniform for all $|t'|$ consistent with pion exchange. The elements Re ρ_{13} and Re ρ_{-31} are also small as required by pion exchange, although the former oscillates and the latter monotonically decreases with $|t|$.

In the reaction

$$\pi^- p \to p\rho^0\pi^- \tag{3}$$

we have limited the analysis to that of the more peripheral ρ by considering only those ρ's formed by π^+ and π_f^-. It is known that there is considerable S-wave background beneath the ρ. This implies that experimentally accessible density matrix elements are $\rho_{00}-\rho_{11}$, ρ_{1-1}, and Re ρ_{10}.

We have calculated these elements in the helicity frame, and have illustrated them in Figs. 9(a)–9(c). For pure pion exchange with the ρ having helicity zero, $\rho_{00}=1$ and the other elements should vanish. We see that for very low $|t'|$, $\rho_{00}-\rho_{11}$ is large and $|\rho_{1-1}|$ and $|\text{Re}\,\rho_{10}|$ are both small. However, the former decreases with $|t'|$ and $|\rho_{11}|$ is larger for larger $|t'|$, implying that pion exchange is dominant (if ρ_{11} is also small) only at small $|t'|$. If we assume that there is no S-wave background then ρ_{00}, Re ρ_{10}, and the combinations $\rho_{11}\pm\rho_{1-1}$ corresponding to natural-parity $(+)$ and unnatural-parity $(-)$ exchanges are accessible and are shown in Fig. 9. We see that ρ_{00} is similar in shape to $\rho_{00}-\rho_{11}$, and the $\rho_{11}\pm\rho_{1-1}$ are small for low $|t'|$ and larger for higher $|t'|$, although $\rho_{11}-\rho_{1-1}$ corresponding to pion exchange with helicity flip at the meson vertex rises more and at lower $|t'|$ than the natural-parity component. Actually, there is considerable S-wave background

which interferes constructively with the P wave, as can be seen in Figs. 9(g) and 9(h). The ρ_{00} interference is considerable, especially at low $|t'|$. All of the matrix elements satisfy the positivity constraints:

$$\rho_{11} \geq |\rho_{1-1}|$$

$$\rho_{00}(\rho_{11}-\rho_{1-1}) \geq 2|\rho_{10}|^2 .$$

We now turn to the reaction

$$\pi^- p \to p f \pi^- , \tag{4}$$

where the situation for the f meson (spin 2) is more complicated because there are now S- and P-wave backgrounds, more positivity constraints, and fewer events in the sample. We have not attempted a likelihood fit to obtain values consistent with the positivity constraints which are, in fact, violated. Our main interest is to show that pion exchange is likely at low $|t'|$. We have again performed the analysis in the helicity frame. Owing to S- and P-wave backgrounds only those matrix elements shown in Figs. 10(a)–10(i) are accessible. Large $\rho_{00}-\rho_{11}$ and $\rho_{00}-\rho_{22}$ do indeed suggest that pion exchange might be important. By assuming pure D wave, we may isolate natural- and unnatural-parity exchanges. The results are shown in Figs. 10(j)–10(r) with the elements in Figs. 10(j)–10(l) corresponding to natural-parity exchange, the remainder to unnatural-parity exchange. We see that pion exchange (large ρ_{00}) falls with $|t'|$ but remains dominant for all $|t'|$.

IV. COMPARISON TO DOUBLE-REGGE MODEL

Having seen hints that quasi-three-body production in our channel has a large contribution from pion exchange, we have attempted to compare a model containing pion exchange to our data. To this end we have used the double-Regge model due to Berger[5] and illustrated diagrammatically for our three final states in Figs. 11(a)–(c). This model has had previous successes. In particular, it has been used to describe $\Delta^{++}\pi^-\pi^-$, $p\rho^0\pi^-$ and $pf\pi^-$ at 6, 13, and 20 GeV/c beam momentum.[4,6] The details of the analysis of these lower-statistics experiments differed from ours (to be described below) but the results are quite insensitive to these differences. These diagrams contain P and π exchanges at the nonresonant and resonant vertices, respectively. We have also examined the model in Figs. 11(b) and 11(c), in which the pion and two-body resonance lines have been switched and the π exchange has been replaced by ρ and f exchange [see Figs. 11(a) and 11(e)]. The matrix elements squared is

$$\sum |M|^2 = G(t_2)(S_2'/S_0)^{2\alpha}(S_1')^2 e^{-a|t_1|} ,$$

$$G(t_2) = \{[1-\tau\cos(\pi\alpha)][(\Gamma(1+\alpha)]^2\}^{-1} ,$$

$$\tau = \pm 1 \text{ for } \begin{bmatrix} \pi f \\ \rho \end{bmatrix} \text{ exchange} ,$$

$$\alpha = (t_2 - m_\pi^2)\alpha' \text{ for } \pi \text{ exchange} , \tag{5}$$

$$\alpha = 0.5 + \alpha' t_2 \text{ for } \rho, f \text{ exchange} ,$$

$$s_2' = s_2 - t_1 - m_b^2 + \tfrac{1}{2}(m_R^2 - t_1 - t_2) ,$$

$$s_1' = s_1 - t_2 - m_a^2 - \tfrac{1}{2}(m_\pi^2 - t_1 - t_2) ,$$

$$\Gamma = \text{ gamma } function .$$

We have fixed the parameters $s_0 = 1.0$ GeV^2, $\alpha' = 1.0$ GeV^2, and $a = 3.5$ GeV^{-2} (5.0 GeV^{-2}) for Δ^{++} (ρ,f) production. The only free parameter is the normalization which we set so that the number of events in the model is the same as the experimental sample used.

In order to be in a region of phase space where the model should apply we have made certain cuts on the data and have applied the same cuts to the Monte Carlo–generated model. These cuts reduce the total number of events that are used to test the model to about 50% of those events containing the two-body resonance. We still are left with a large sample due to high statistics. These cuts are given in Table VI. They tend to emphasize the peripherality of the reaction, as well as to enhance the π exchange with respect to the Regge exchange or *vice versa*. In particular, it has been shown[7] that by constraining the azimuthal angle ϕ_H of the two-body resonance in the three-body helicity rest frame pion exchange is enhanced. We have included this constraint for Δ^{++} production. For ρ and f production we have enhanced π exchange by restricting events to those where the magnitude of the four-momentum transfer between beam and resonance is smaller than that between beam and π^-.

We have plotted our results for Δ^{++} production from reaction (2) with π and P exchanges in Figs. 12(a)–12(c). As is known, there are only four independent variables for a three-body final state up to a general rotation. Thus, the nine variables that appear are correlated. We recall that in the data the resonances are defined by mass cuts and there is only one free parameter in this and the following figures, which all include the three possible

effective-mass plots, $|t_1|$, $|t_2|$, and the cosine of the polar angle and the azimuthal angle in each of the two Gottfried-Jackson frames containing the central outgoing meson. We see that the $\Delta^{++}\pi^-$ low-mass enhancement from the model is slightly shifted to higher mass to that of the data. The model predicts a peaking at a higher value of $\pi^-\pi^-$ mass than the data indicate. The $|t|$ and angular distributions describe the data well. The overall prediction of the model is good.

The comparison between the model and the data for ρ production from reaction (3) is given in Figs. 13 and 14, the former for π,P exchanges, the latter for ρP exchanges. Again, for both processes there is overall agreement between the data and the model. Both exchanges predict the A_1 [Figs. 13(c) and 14(c)], the π exchange process predicting a narrower A_1 than the data show and the ρ exchange predicting a broader and lower A_1 than the experiment. We do note that neither model can account for the A_2. This is probably due to direct production of A_2 which proceeds via ρ exchange. Whereas the π exchange model seems to be somewhat more peripheral than the data at the meson vertex, the ρ exchange model seems less peripheral than the data as can be seen from Figs. 13(d) and 13(e) and 14(d) and 14(e). The ρ-exchange model fails to account for the azimuthal distributions. This failure may indicate that other Regge exchanges and/or cuts also contribute in the region of phase space under consideration.

We have performed a similar analysis for f production from reaction (4) via π,P and via f,P exchanges, with the results shown in Figs. 15 and 16, for the respective exchanges. In the latter case we have removed events with effective mass in the Δ^{++} mass region in order to remove the Δ^{++} reflection in the 2.3—2.4 GeV region of the $f\pi$ mass spectrum. The A_3 peak is evident in both models, although it is at a lower mass than the data indicate for πP exchange. Most other spectra are well described by the model.

V. CONCLUDING REMARKS

We have done a study with large statistics from the reaction $\pi^-p\to\pi^-\pi^+\pi^-p$ at 8-GeV/c beam momentum. This reaction is dominated by production of ρ and Δ^{++} resonances with considerable f and Δ^0 production. A fair amount of this resonance production results from the decay of A_1, A_2, A_3, and $N(1470)$ enhancements. Evidence for double-resonance production of $\rho^0\Delta^0$, $f\Delta^0$, $\rho^0N(1520)$, and $\rho^0N(1688)$ has been found. The reaction is peripheral with the slope of the t' distribution of the diffractive enhancement falling with the mass of the enhancement. Quasi-three-body production of Δ^{++} is well described by a double-Regge model with π and P exchanges at the vertices. Such exchanges also describe a great deal of ρ and f quasi-three-body production. A good portion of the remainder of this production is in agreement with the same type of model, but with ρ and P exchanges (ρ production) or f and P exchanges (f production).

ACKNOWLEDGMENTS

This work was supported in part by the United States Department of Energy, the National Science Foundation, and the Japan Society for the Promotion of Science. We wish to thank the SLAC bubble-chamber operating crew for its professional operation of the bubble chamber and the quality of the film. We also wish to thank the data-reduction teams at Tohoku University, Massachussetts Institute of Technology, Oak Ridge National Laboratory, and the University of Tennessee, whose dedicated efforts made this experiment possible.

---

[a]Now at Heidelberg University, West Germany.
[b]Now at Tufts University, Medford, Massachusetts 02155.
[c]Now at Mitsui-Joho KK, Tokyo, Japan.
[d]Now at DESY, Hamburg, West Germany.
[e]Permanent address: Tel-Aviv University, Ramat-Aviv, Israel.
[f]Now at SLAC, Stanford, California 94305.
[g]Permanent address: Istituto di Física Nucleare, Pavia, Italy.
[h]Now at Weizmann Institute, Rehovot, Israel.
[i]Now at CERN, Geneva 23, Switzerland.
[j]Permanent address: Nara Women's University, Nara, Japan.
[k]Now at Rockefeller University, New York, New York 10021.
[l]Now at Automatix, Burlington, Massachusetts 01803.
[m]Now at Bell Laboratories, Naperville, Illinois 60540.
[n]Permanent address: Inst. of High Energy Physics, Beijing, China.

[1]Particle Data Group, Report No. LBL-90, 1978 (unpublished and references cited therein).

[2]J. W. Lamsa *et al.*, Phys. Rev. 166, 1395 (1968).
[3]E. Bracci *et al.*, Report No. CERN/HERA 72-1 (unpublished).
[4]K. F. Galloway *et al.*, Phys. Rev. D 1, 3077 (1970); S. Miyashita *et al.*, *ibid.* 1, 771 (1970); N. Cason *et al.*, Phys. Rev. 148, 1282 (1966); N. Biswas *et al.*, *ibid.* 134, 901 (1964).
[5]E. L. Berger, Phys. Rev. 179, 1567 (1969).
[6]G. W. Brandenburg *et al.*, Nucl. Phys. B16, 369 (1970).
[7]E. L. Berger, Phys. Rev. D 11, 3214 (1975).